JOURNAL OF AIRCRAFT
Vol. 46, No. 4, July–August 2009

Active Control of Vertical Tail Buffeting by Piezoelectric Actuators

Y. H. Zhao* and H. Y. Hu†
Nanjing University of Aeronautics and Astronautics, 210016 Nanjing, People's Republic of China

DOI: 10.2514/1.39464

A simplified method for analyzing and designing a vertical tail buffeting alleviation system is developed. The vertical tail model in this study is equipped with surface-bonded piezoelectric actuators to suppress the buffeting responses induced by aerodynamic forces. The structural dynamics of the vertical tail and the electrodynamics of piezoelectric actuators are modeled using a finite element method and realized by commercial software packages ANSYS®. Afterward, the finite element model for both the host structure and the piezoelectric patches are imported into MATLAB®, in which the dynamic equations of the system in modal coordinates are obtained through modal truncation. The motion-induced aerodynamic forces are computed by using the doublet-lattice method. The buffet input excitations are simulated by the proper orthogonal decomposition-based method. The suboptimal controller is designed to compute suitable control voltages needed to drive piezoelectric actuators. Finally, the effectiveness of the piezoelectric actuators in reducing vibratory responses due to buffet loads on the vertical tail is investigated numerically. The results demonstrate that the proposed method is feasible and effective.

Nomenclature

b_R	=	reference half-chord length
$\boldsymbol{C}_{aw}$	=	output matrix
$\boldsymbol{c}^E$	=	stiffness matrix evaluated at constant electric field
$\boldsymbol{C}_{uu}$	=	structural damping matrix
$\boldsymbol{D}$	=	electric displacement vector
$\boldsymbol{d}$	=	piezoelectric matrix relating strain/electric field
$\boldsymbol{E}$	=	electric field vector
E_e	=	Young's modulus of elasticity
$\boldsymbol{e}$	=	piezoelectric matrix relating stress/electric field
$\bar{\boldsymbol{F}}_{bs}$	=	modal forces of the random buffet excitation
$\boldsymbol{F}_u$	=	external forces
$\bar{\boldsymbol{F}}_{us}$	=	modal force vector of the motion-induced aerodynamic loads
$\boldsymbol{F}_\varphi$	=	external electric charges
$\boldsymbol{H}_{FW}(s)$	=	transfer function
$\boldsymbol{K}_{\text{con}}$	=	control gain
$\boldsymbol{K}_{uu}$	=	structural stiffness matrix
$\boldsymbol{K}_{u\varphi}$	=	piezoelectric coupling matrix
$\boldsymbol{K}_{\varphi\varphi}$	=	dielectric stiffness matrix
k	=	reduced frequency
$\boldsymbol{M}_{uu}$	=	structural mass matrix
M_∞	=	Mach number
n_r	=	number of the retained structural modes
n_w	=	dimensions of the state vector $\boldsymbol{X}_w(t)$
p_{bu}	=	aerodynamic pressure due to buffet
p_{us}	=	unsteady aerodynamic pressure
$\boldsymbol{Q}$	=	modal coordinate
$\bar{\boldsymbol{Q}}$	=	state penalty matrix
$\boldsymbol{Q}_{uu}(M_\infty, k)$	=	generalized aerodynamic matrix
q_d	=	dynamic pressure
$\boldsymbol{R}$	=	control penalty and state penalty matrix,
$\boldsymbol{S}$	=	strain vector
$\boldsymbol{S}_E$	=	compliance matrix evaluated at constant electric field
$\boldsymbol{S}_{FF}(\omega)$	=	cross-power spectral density matrix of the buffet loads
$\boldsymbol{S}_v$	=	matrix for which the elements are related to the locations of sensors
s	=	Laplace variable
$\boldsymbol{T}_{FY}(s)$	=	transfer function of the correlating filter $\Re$
$\boldsymbol{T}_{YW}(s)$	=	transfer function of the colorizing filter M
$\boldsymbol{u}$	=	structural displacement
V	=	airspeed
$\boldsymbol{V}_{\text{con}}$	=	control voltage
$\boldsymbol{W}_w(t)$	=	vector of Gaussian, independent, unit-intensity white noise
$\boldsymbol{X}_w(t)$	=	state vector
$\boldsymbol{Y}_{ae}(t)$	=	measured velocity output
$\boldsymbol{\varepsilon}^S$	=	dielectric matrix evaluated at constant strain
$\boldsymbol{\varepsilon}^\sigma$	=	dielectric matrix evaluated at constant stress
υ	=	Poisson's ratio
ρ	=	vertical tail density
$\boldsymbol{\sigma}$	=	stress vector
$\boldsymbol{\Phi}$	=	truncated modal matrix
$\boldsymbol{\varphi}$	=	electric potential vector
$\boldsymbol{\Psi}(\omega)$	=	modal matrix of $\boldsymbol{S}_{FF}(\omega)$, for which the columns are eigenvectors of $\boldsymbol{S}_{FF}(\omega)$
ω	=	angular frequency

I. Introduction

THE capability of modern fighter aircraft to sustain high angles of attack often results in immersion of part of the aircraft in unsteady, separated, vortical flow emanating from the aircraft's forebody or wings. The vortices from these surfaces break down upstream of the vertical tails. This flow contains significant levels of energy over a frequency bandwidth coincident with low-order structural vibration modes of the tails, and therefore vertical tail buffeting occurs. Some consequences of buffeting are the premature initiation of fatigue cracks. Initiation and growth of these fatigue cracks result in more frequent inspections of the aircraft and additional repairs or replacement of vertical tails. In addition to the formation of fatigue cracks, buffet-induced vibrations can restrict the flight maneuvering capability of the aircraft by restricting the angles of attack and speeds at which certain maneuvers can be executed [1].

Many different approaches to tail buffeting alleviation have been investigated. These approaches can be divided into two sets: the

Received 30 June 2008; revision received 8 February 2009; accepted for publication 2 April 2009.

*Associate Professor, Institute of Vibration Engineering Research; zyhae@nuaa.edu.cn (Corresponding Author).

†Professor, Institute of Vibration Engineering Research.

aerodynamic methods and structural dynamic methods. Aerodynamic approaches can be further divided into passive and active methods for reducing the strength or for delaying the formation of the vortices. The passive aerodynamic approach consists of adding fences on the wing or the fuselage. The leading-edge extension fences on the F/A-18 aircraft are examples of such devices. Usually, active aerodynamic methods are based on tangential leading-edge blowing (TLEB). The application of TLEB for fin buffeting alleviation has been studied on single-fin aircraft [2] and twin-tail aircraft [3]. The structural dynamic methods for buffet alleviation can also be divided into passive and active approaches. The passive structural approach consists of reinforcing of the fin assembly with patches both to repair existing defects and to stiffen the assembly. These passive techniques have been successful at reducing the buffeting response of the vertical tails but have increased gross weight of the vehicle.

In recent years, active structural control techniques have been investigated. Lazarus et al. [4] numerically studied the feasibility of using an active piezoelectric buffeting suppression system. This system, called the buffeting load alleviation, consists of a large number of piezoceramic wafer actuators, strain gauges, and accelerometers as sensors and linear quadratic Gaussian (LQG) design for the controller. Recently, Spangler and Jacques [5] have experimentally tested this buffeting load alleviation system on a full-scale F/A-18 empennage, showing that their system could reduce the root-mean-square (rms) strain at the aft root of the vertical tail by up to 50%. Hauch et al. [6] developed an active vertical tail to study the feasibility of buffeting alleviation using piezoceramic actuators, strain gauge sensors, and simple control techniques. Nitzsche et al. [7] compared the two different approaches of using an aerodynamic control surface or using piezoceramic actuators for tail buffeting alleviation. Using LQG controllers, their simulations [7] showed that the strain actuation approach would appear to demonstrate a better performance. Then Nitzsche et al. [8] tested their LQG controller on a full-scale F/A-18 empennage with strain actuation, showing reduction of buffeting vibrations by up to 58%. As part of the actively controlled response of buffet-affected tails (ACROBAT) program, Moses [9] performed wind-tunnel tests on a 1/6-scale F/A-18 aircraft. The buffeting alleviation controller, which was based on frequency-domain compensation methods, was designed to suppress the response in the first bending mode of the tail using either the rudder or some piezoceramic actuators and an accelerometer as the sensor. The wind-tunnel tests showed that using the rudder as the control actuator provided less alleviation than using piezoceramic actuators. Sheta and Moses [10] numerically investigated piezoceramic actuators installed on the inboard and outboard surfaces of the vertical tail of an F/A-18 to control the buffeting responses in the first bending and torsion modes. A single-input/single-output controller is designed to drive the active piezoelectric actuators. A multidisciplinary analysis was performed, taking into account the fluid dynamics, structure dynamics, electrodynamics of the piezoelectric actuators, fluid–structure interfacing, and grid motion, which are integrated into a multidisciplinary computing environment that controls the temporal synchronization of the analysis. The results show that the peak values of the power spectral density (PSD) of tail tip acceleration are reduced by as much as 22% in the first bending mode and by as much as 82% in the first torsion mode. The rms values of tip acceleration are reduced by as much as 12%.

In the previous studies, the structural modeling methods for the vertical-tail/piezoelectric-actuator system have not been described in detail. In addition, the procedure for predicting buffet loads by solving the full Navier–Stokes equations is very complicated and time-consuming. Therefore, the simplified structural and the aerodynamic modeling methods are needed from a practical point of view. In fact, the commercial software packages ANSYS® has the ability to model 3-D piezoelectric materials. Hence, the basic ideal of this paper is that the structural model of the vertical-tail/piezoelectric-actuator system is modeled in the ANSYS platform. Then the finite element matrices are imported into MATLAB® for the designing of the controller. The unsteady aerodynamic loads due to the motion of the tail are modeled by using the doublet-lattice method (DLM), and buffet loads are generated by proper orthogonal decomposition-based (POD) method. The suboptimal controller is designed. The effectiveness of the piezoelectric actuator in buffeting alleviation of the vertical tail is demonstrated by numerical simulations.

II. Finite Element Modeling

In this section, a 3-D finite element model of the vertical tail with piezoelectric patches are modeled by using the commercial software packages ANSYS. Then all of the finite element matrices are imported into MATLAB. The equations of motion for the present structural system in modal space are obtained.

A. Constitutive Equations

The subject of study in this effort is an isolated vertical tail. A cross-section schematic is shown in Fig. 1. Nine piezoelectric actuators are bonded on the one side of the vertical tail. The constitutive equations given by manufacturers or published data are usually in the following form:

$$\boldsymbol{S} = \boldsymbol{s}^E\boldsymbol{\sigma} + \boldsymbol{d}\boldsymbol{E} \tag{1}$$

$$\boldsymbol{D} = \boldsymbol{d}^T\boldsymbol{\sigma} + \boldsymbol{\varepsilon}^\sigma\boldsymbol{E} \tag{2}$$

where $\boldsymbol{\sigma}$ is the stress vector, $\boldsymbol{S}$ is the strain vector, $\boldsymbol{D}$ is the electric displacement vector, $\boldsymbol{E}$ is the electric field vector, $\boldsymbol{s}^E$ is the compliance matrix evaluated at constant electric field, $\boldsymbol{d}$ is the piezoelectric matrix relating strain/electric field, $\boldsymbol{d}^T$ is the transpose of matrix $\boldsymbol{d}$, and $\boldsymbol{\varepsilon}^\sigma$ is the dielectric matrix evaluated at constant stress. However, ANSYS requires data in the following form:

$$\boldsymbol{\sigma} = \boldsymbol{c}^E\boldsymbol{S} - \boldsymbol{e}\boldsymbol{E} \tag{3}$$

$$\boldsymbol{D} = \boldsymbol{e}^T\boldsymbol{S} + \boldsymbol{\varepsilon}^S\boldsymbol{E} \tag{4}$$

where $\boldsymbol{c}^E$ is the stiffness matrix evaluated at constant electric field, $\boldsymbol{e}$ is the piezoelectric matrix relating stress/electric field, $\boldsymbol{e}^T$ is the transpose of matrix $\boldsymbol{e}$, and $\boldsymbol{\varepsilon}^S$ is the dielectric matrix evaluated at constant strain. Note that piezoelectric matrix $\boldsymbol{e}$ accounts for the piezoelectric effect (i.e., the intrinsic coupling between mechanical and electric fields). Equation (3) characterizes the converse piezoelectric effect that enables piezoelectric materials to function as actuators, and Eq. (4) characterizes the direct piezoelectric effect that enables piezoelectric materials to function as sensors.

To convert the manufacturer's data presented in the form of Eqs. (1) and (2) to ANSYS notation [Eqs. (3) and (4)], one can use the following relationship between manufacturer-supplied data and ANSYS-required values, given by

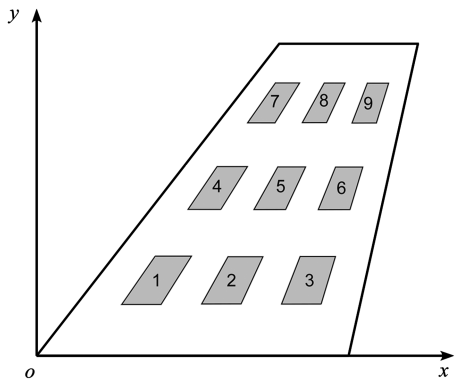

Fig. 1 Cross section of the vertical tail used for analysis.

$$\begin{cases} \boldsymbol{c}^E = (\boldsymbol{s}^E)^{-1} \\ \boldsymbol{\varepsilon}^S = \boldsymbol{\varepsilon}^\sigma - \boldsymbol{d}^t(\boldsymbol{s}^E)^{-1}\boldsymbol{d} \\ \boldsymbol{e} = (\boldsymbol{s}^E)^{-1}\boldsymbol{d} \end{cases} \tag{5}$$

The top and bottom surfaces of the piezoelectric actuators are electroded. The electroded regions represent equipotential surfaces. The bottom electrodes of the piezoelectric actuators are grounded (voltages are set equal to zero). The theoretical studies regarding modeling and design of smart structures are performed by using the finite element method, which is shown to be a very effective tool for the analysis of piezoelectric materials, as the method offers fully coupled thermomechanical-electrical analysis of structures. It is assumed that the thermal effect is not considered in the analysis.

B. Electromechanically Coupled System

Variational principles can be used to establish the finite element equations for piezoelectric structure. The global equation of motion governing the vertical tail system with piezoelectric actuators can be written as

$$\begin{bmatrix} \boldsymbol{M}_{uu} & 0 \\ 0 & 0 \end{bmatrix} \begin{Bmatrix} \ddot{\boldsymbol{u}} \\ \ddot{\boldsymbol{\varphi}} \end{Bmatrix} + \begin{bmatrix} \boldsymbol{C}_{uu} & 0 \\ 0 & 0 \end{bmatrix} \begin{Bmatrix} \dot{\boldsymbol{u}} \\ \dot{\boldsymbol{\varphi}} \end{Bmatrix} + \begin{bmatrix} \boldsymbol{K}_{uu} & \boldsymbol{K}_{u\varphi} \\ \boldsymbol{K}_{u\varphi}^T & \boldsymbol{K}_{\varphi\varphi} \end{bmatrix} \begin{Bmatrix} \boldsymbol{u} \\ \boldsymbol{\varphi} \end{Bmatrix} = \begin{Bmatrix} \boldsymbol{F}_u \\ \boldsymbol{F}_\varphi \end{Bmatrix} \tag{6}$$

where $\boldsymbol{u}$ denotes structural displacement, $\boldsymbol{\varphi}$ denotes electric potential vector, $\boldsymbol{M}_{uu}$ is the structural mass matrix, $\boldsymbol{C}_{uu}$ is the structural damping matrix, $\boldsymbol{K}_{uu}$ is the structural stiffness matrix, $\boldsymbol{K}_{u\varphi}$ is the piezoelectric coupling matrix, $\boldsymbol{K}_{\varphi\varphi}$ is the dielectric stiffness matrix, and a superscript T denotes transpose of a matrix, $\boldsymbol{F}_u$ denotes the external forces, and $\boldsymbol{F}_\varphi$ denotes external electric charges. Electric potential vector $\boldsymbol{\varphi}$ of the top electrodes of piezoelectric actuators can be written as

$$\boldsymbol{\varphi} = \begin{Bmatrix} \boldsymbol{\varphi}_1 \\ \boldsymbol{\varphi}_2 \\ \vdots \\ \boldsymbol{\varphi}_m \end{Bmatrix}, \qquad \boldsymbol{\varphi}_j = \begin{Bmatrix} \varphi_{j(1)} \\ \varphi_{j(2)} \\ \vdots \\ \varphi_{j(n)} \end{Bmatrix} \tag{7}$$

where $\boldsymbol{\varphi}_j$ $(j = 1, \ldots, m)$ denotes the electric potential vector of the nodes on the top electrode of the jth piezoelectric patch, m is the number of the actuators, and n is the number of the nodes on the top electrode of each patch.

C. Equations of Motion in Modal Space

Structural damping matrix $\boldsymbol{C}_{uu}$ is usually assumed to be a linear combination of the structural mass matrix $\boldsymbol{M}_{uu}$ and the structural stiffness matrix $\boldsymbol{K}_{uu}$, given by

$$\boldsymbol{C}_{uu} = a\boldsymbol{M}_{uu} + b\boldsymbol{K}_{uu} \tag{8}$$

where the constants a and b are experimentally determined. Aerodynamic damping is inherited in the aeroelastic model when aerodynamic loads are considered.

For the vertical tail buffeting alleviation applications, the electric potential vector $\boldsymbol{\varphi}$ is controlled; in this case, the governing equations of the smart vertical tail system become

$$\boldsymbol{M}_{uu}\ddot{\boldsymbol{u}} + \boldsymbol{C}_{uu}\dot{\boldsymbol{u}} + \boldsymbol{K}_{uu}\boldsymbol{u} = \boldsymbol{F}_u - \boldsymbol{K}_{u\varphi}\boldsymbol{\varphi} \tag{9}$$

Because all of the nodes on one electrode surface have identical potentials, one has

$$\varphi_{j(1)} = \varphi_{j(2)} = \cdots = \varphi_{j(n)} = V_j, \quad j = 1, \ldots, m \tag{10}$$

From Eqs. (7) and (10), we have the following relationship between electric potential $\boldsymbol{\varphi}$ and control voltage $\boldsymbol{V}_{\text{con}}$:

$$\boldsymbol{\varphi} = \boldsymbol{T}_v \boldsymbol{V}_{\text{con}} \tag{11}$$

where

$$\boldsymbol{T}_v = \begin{bmatrix} \boldsymbol{\alpha}_v & 0 & \cdots & 0 \\ 0 & \boldsymbol{\alpha}_v & \cdots & 0 \\ 0 & \vdots & \ddots & \vdots \\ 0 & 0 & \cdots & \boldsymbol{\alpha}_v \end{bmatrix}, \qquad \boldsymbol{\alpha}_v = \begin{Bmatrix} 1 \\ 1 \\ \vdots \\ 1 \end{Bmatrix}_{n\times 1}$$
$$\boldsymbol{V}_{\text{con}} = \begin{Bmatrix} V_1 \\ V_2 \\ \vdots \\ V_m \end{Bmatrix} \tag{12}$$

Substituting Eq. (11) into Eq. (9), we obtain

$$\boldsymbol{M}_{uu}\ddot{\boldsymbol{u}} + \boldsymbol{C}_{uu}\dot{\boldsymbol{u}} + \boldsymbol{K}_{uu}\boldsymbol{u} = \boldsymbol{F}_u - \boldsymbol{K}_{u\varphi}\boldsymbol{T}_v\boldsymbol{V}_{\text{con}} \tag{13}$$

Note that the second term in the right-hand side of Eq. (13) represents the equivalent piezoelectric loads. From Eq. (13), we can see that the eigenvalues problem of the system (structural damping is neglected) with short-circuited electrodes ($\boldsymbol{V}_{\text{con}} = 0$) is

$$(\boldsymbol{K}_{uu} - \omega^2\boldsymbol{M}_{uu})\boldsymbol{\Phi} = 0 \tag{14}$$

Note that the natural frequencies and modal shape are the same as when there is no piezoelectric electromechanical coupling. To obtain a reduced-order model, modal transformation and truncation of high-frequency modes are performed. Thus, Eq. (13) can be rewritten in modal space form as

$$\bar{\boldsymbol{M}}_{uu}\ddot{\boldsymbol{q}} + \bar{\boldsymbol{C}}_{uu}\dot{\boldsymbol{q}} + \bar{\boldsymbol{K}}_{uu}\boldsymbol{q} = \bar{\boldsymbol{F}}_u - \bar{\boldsymbol{K}}_{u\varphi}\boldsymbol{V}_{\text{con}} \tag{15}$$

where

$$\bar{\boldsymbol{M}}_{uu} = \boldsymbol{\Phi}^T\boldsymbol{M}_{uu}\boldsymbol{\Phi}, \qquad \bar{\boldsymbol{C}}_{uu} = \boldsymbol{\Phi}^T\boldsymbol{C}_{uu}\boldsymbol{\Phi}, \qquad \bar{\boldsymbol{K}}_{uu} = \boldsymbol{\Phi}^T\boldsymbol{K}_{uu}\boldsymbol{\Phi} \tag{16}$$

$$\bar{\boldsymbol{F}}_u = \boldsymbol{\Phi}^T\boldsymbol{F}_u, \qquad \bar{\boldsymbol{K}}_{u\varphi} = \boldsymbol{\Phi}^T\boldsymbol{K}_{u\varphi}\boldsymbol{T}_v \tag{17}$$

where $\boldsymbol{\Phi}$ is the truncated modal matrix and $\boldsymbol{q}$ is the modal coordinate.

III. Open-Loop Aeroelastic Equations

In this section, unsteady aerodynamic forces acting on the vertical wing are computed by DLM. The minimum state method is used to transform the obtained aerodynamic forces from the reduced frequency domain to the Laplace domain. Finally, the open-loop aeroelastic equations of the system are obtained.

A. Minimum State Approximation

Let the component of the loads due to unsteady aerodynamic pressure be represented by $p_{us}(x, y, t)$ and that due to buffet be $p_{bu}(x, y, t)$. We assume that aerodynamic forces acting on the vertical tail surface can be represented by the addition of the two forces as follows [11]:

$$p_u(x, y, t) = p_{us}(x, y, t) + p_{bu}(x, y, t) \tag{18}$$

The first term in the right-hand side of Eq. (18) denotes the motion-induced aerodynamic forces, the second term denotes random buffet input excitation usually obtained from rigid-model pressure measurements due to flow separation. Obviously, the total aerodynamic forces $\bar{\boldsymbol{F}}_u$ in modal space can be written as

$$\bar{\boldsymbol{F}}_u = \bar{\boldsymbol{F}}_{us} + \bar{\boldsymbol{F}}_{bs} \tag{19}$$

where $\bar{\boldsymbol{F}}_{us}$ is the modal force vector of the motion-induced aerodynamic loads, and $\bar{\boldsymbol{F}}_{bs}$ are the modal forces of the random buffet excitation.

The DLM can be used to compute motion-induced aerodynamic forces [12]. In the modal space, the generalized aerodynamic forces can be expressed as

$$\bar{\boldsymbol{F}}_{us} = q_d \boldsymbol{Q}_{uu}(M_\infty, k)\boldsymbol{q} \tag{20}$$

where q_d is the dynamic pressure, $\boldsymbol{Q}_{uu}(M_\infty, k)$ is the generalized aerodynamic matrix, M_∞ is the Mach number, and k is the reduced frequency.

The aerodynamic force are approximated as the transfer functions of the Laplace variable by a nonlinear least-squares curve-fit approximation to define the equations of motion in a linear time-invariant state-space form. Here, the minimum state method is used for rational function approximation of the generalized aerodynamic matrix $\boldsymbol{Q}_{uu}(M_\infty, k)$. Thus, Eq. (15) can be written as

$$\begin{aligned}\bar{\boldsymbol{M}}_{uu}\ddot{\boldsymbol{q}} + \bar{\boldsymbol{C}}_{uu}\dot{\boldsymbol{q}} + \bar{\boldsymbol{K}}_{uu}\boldsymbol{q} - q_d(\boldsymbol{A}_0 + \boldsymbol{A}_1\bar{s} + \boldsymbol{A}_2\bar{s}^2 \\ + \boldsymbol{D}_s(\boldsymbol{I}\bar{s} - \boldsymbol{R}_s)^{-1}\boldsymbol{E}_s\bar{s})\boldsymbol{q} = \bar{\boldsymbol{F}}_{bs} - \bar{\boldsymbol{K}}_{u\varphi}\boldsymbol{V}_{\text{con}}\end{aligned} \tag{21}$$

where $\bar{s} = sb_R/V = ik$, s is the Laplace variable, b_R is the reference half-chord length, V is the airspeed, and $i = \sqrt{-1}$.

B. Open-Loop State-Space Equations

Introducing the aerodynamic states $\boldsymbol{q}_a$ as follows,

$$\boldsymbol{q}_a = (\boldsymbol{I}\bar{s} - \boldsymbol{R}_s)^{-1}\boldsymbol{E}_s\bar{s}\boldsymbol{q} \tag{22}$$

Substituting Eq. (22) into Eq. (21), we have

$$\bar{\bar{\boldsymbol{M}}}_{uu}\ddot{\boldsymbol{q}} = -\bar{\bar{\boldsymbol{C}}}_{uu}\dot{\boldsymbol{q}} - \bar{\bar{\boldsymbol{K}}}_{uu}\boldsymbol{q} + q_d\boldsymbol{D}_s\boldsymbol{q}_a + \bar{\boldsymbol{F}}_{bs} - \bar{\boldsymbol{K}}_{u\varphi}\boldsymbol{V}_{\text{con}} \tag{23}$$

where

$$\bar{\bar{\boldsymbol{M}}}_{uu} = \bar{\boldsymbol{M}}_{uu} - q_d\left(\frac{b_R}{V}\right)^2\boldsymbol{A}_2, \qquad \bar{\bar{\boldsymbol{C}}}_{uu} = \bar{\boldsymbol{C}}_{uu} - q_d\frac{b_R}{V}\boldsymbol{A}_1 \tag{24}$$

$$\bar{\bar{\boldsymbol{K}}}_{uu} = \bar{\boldsymbol{K}}_{uu} - q_d\boldsymbol{A}_0 \tag{25}$$

From Eq. (22), we see that the aerodynamic states $\boldsymbol{q}_a$ satisfy the following equation:

$$\dot{\boldsymbol{q}}_a = \boldsymbol{R}_s\frac{V}{b}\boldsymbol{q}_a + \boldsymbol{E}_s\dot{\boldsymbol{q}} \tag{26}$$

So the aeroelastic equation of the open-loop system can be written as

$$\dot{\boldsymbol{X}}_a(t) = \boldsymbol{A}_a\boldsymbol{X}_a(t) + \boldsymbol{B}_a\boldsymbol{V}_{\text{con}}(t) + \boldsymbol{D}_a\bar{\boldsymbol{F}}_{bs}(t) \tag{27}$$

where

$$\boldsymbol{A}_a = \begin{bmatrix} 0 & \boldsymbol{I} & 0 \\ -\bar{\bar{\boldsymbol{M}}}_{uu}^{-1}\bar{\bar{\boldsymbol{K}}}_{uu} & -\bar{\bar{\boldsymbol{M}}}_{uu}^{-1}\bar{\bar{\boldsymbol{C}}}_{uu} & q_d\bar{\bar{\boldsymbol{M}}}_{uu}^{-1}\boldsymbol{D}_s \\ 0 & \boldsymbol{E}_s & (V/b_R)\boldsymbol{R}_s \end{bmatrix} \tag{28}$$

$$\boldsymbol{B}_a = \begin{Bmatrix} 0 \\ -\bar{\bar{\boldsymbol{M}}}_{uu}^{-1}\bar{\boldsymbol{K}}_{u\varphi} \\ 0 \end{Bmatrix}, \qquad \boldsymbol{D}_a = \begin{Bmatrix} 0 \\ \bar{\bar{\boldsymbol{M}}}_{uu}^{-1} \\ 0 \end{Bmatrix} \tag{29}$$

$$\boldsymbol{X}_a(t) = \begin{Bmatrix} \boldsymbol{q} \\ \dot{\boldsymbol{q}} \\ \boldsymbol{q}_a \end{Bmatrix} \tag{30}$$

IV. State-Space Model of the Buffet Loads

It is well known that the buffet loads are difficult to be predicted exactly by numerical simulations, due to their random nature. Therefore, a buffeting prediction technique based on rigid-model pressure measurement is commonly used. A reliable way to obtain the buffet loads is based on the wind-tunnel testing for the rigid tail. If the cross-power spectral density matrix of the buffet loads on the selected key points is obtained from rigid-model pressure measurement, then the state-space model of the buffet loads can be obtained by the POD method.

A. Proper Orthogonal Decomposition

Random buffet loads on the vertical tail can be idealized as a discrete zeros-mean vector-valued stationary random process, denoted by

$$\boldsymbol{F}_{bs}(t) = [\,f_1(t) \quad f_2(t) \quad \cdots \quad f_N(t)\,]^T$$

where $f_1(t), f_2(t), \ldots, f_N(t)$ represent nodal random loads. For the given cross-power spectral density matrix $\boldsymbol{S}_{\boldsymbol{FF}}(\omega)$ of the buffet loads, the POD method given in [13] provides efficient tools to formulate a model of random field based on principal components.

Let $\boldsymbol{\Psi}(\omega)$ be the eigenmatrix of $\boldsymbol{S}_{\boldsymbol{FF}}(\omega)$, for which the columns are eigenvectors of $\boldsymbol{S}_{\boldsymbol{FF}}(\omega)$, normalized with respect to the identity matrix. Then the following relationships hold:

$$\boldsymbol{S}_{\boldsymbol{FF}}(\omega) = \boldsymbol{\Psi}(\omega)\boldsymbol{\Lambda}(\omega)\boldsymbol{\Psi}^*(\omega), \qquad \boldsymbol{\Psi}^*(\omega)\boldsymbol{\Psi}(\omega) = \boldsymbol{I} \tag{31}$$

where

$$\boldsymbol{\Psi}(\omega) = [\,\boldsymbol{\Psi}_1(\omega) \quad \boldsymbol{\Psi}_2(\omega) \quad \cdots \quad \boldsymbol{\Psi}_N(\omega)\,] \tag{32}$$

$$\boldsymbol{\Lambda}(\omega) = \text{diag}[\,\lambda_1 \quad \lambda_2 \quad \cdots \quad \lambda_N\,] \tag{33}$$

The superscript * means the conjugate transpose, $\boldsymbol{\Lambda}(\omega)$ is a diagonal matrix for which the diagonal elements are eigenvalues λ_j associated with $\boldsymbol{\Psi}_j(\omega)$, and $\boldsymbol{S}_{\boldsymbol{FF}}(\omega)$ is Hermitian and nonnegative definite.

Based on the theory of random process, random loads $\boldsymbol{F}_{bs}(t)$ can be regarded as the output of a system with white-noise input: that is,

$$\boldsymbol{F}_{bs}(t) = \Re[\mathsf{M}[\boldsymbol{W}_w(t)]] = \wp[\boldsymbol{W}_w(t)] \tag{34}$$

where $\boldsymbol{W}_w(t)$ is a vector of Gaussian, independent, unit-intensity white noise. The operator M is called the colorizing filter, and operator $\Re$ is called the correlating filter [14]. The transfer function $\boldsymbol{T}_{\boldsymbol{FY}}(s)$ of the correlating filter $\Re$ along the imaginary is determined by the relationship

$$\boldsymbol{T}_{FY}(i\omega) = \boldsymbol{\Psi}(\omega) \tag{35}$$

The transfer function $\boldsymbol{T}_{\boldsymbol{YW}}(s)$ of the colorizing filter M along the imaginary is determined by

$$\boldsymbol{T}_{\boldsymbol{YW}}(i\omega)\boldsymbol{T}^*_{\boldsymbol{YW}}(i\omega) = \boldsymbol{\Lambda}(\omega) \tag{36}$$

Thus, the transfer function of the operator $\wp$ can be written as

$$\boldsymbol{H}_{\boldsymbol{FW}}(s) = \boldsymbol{T}_{\boldsymbol{FY}}(s)\boldsymbol{T}_{\boldsymbol{YW}}(s) \tag{37}$$

From Eqs. (35–37), we have

$$\begin{aligned}\boldsymbol{H}_{\boldsymbol{FW}}(i\omega)\boldsymbol{H}^*_{\boldsymbol{FW}}(i\omega) &= \boldsymbol{T}_{\boldsymbol{FY}}(i\omega)\boldsymbol{T}_{\boldsymbol{YW}}(i\omega)\boldsymbol{T}^*_{\boldsymbol{YW}}(i\omega)\boldsymbol{T}^*_{\boldsymbol{FY}}(i\omega) \\ &= \boldsymbol{\Psi}(\omega)\boldsymbol{\Lambda}(\omega)\boldsymbol{\Psi}^*(\omega)\end{aligned} \tag{38}$$

B. State-Space Model of the Random Buffet Forces

In the POD method, only a limited number ($\bar{N} < N$) of modes are retained in Eq. (31); this is similar to the mode truncation in the structural dynamic analysis. As a result, matrix $\boldsymbol{\Lambda}(\omega)$ is reduced to an $\bar{N}$-order diagonal matrix containing the $\bar{N}$ largest eigenvalues, and $\boldsymbol{\Psi}(\omega)$ is reduced to an $(N \cdot \bar{N})$-order matrix containing the corresponding eigenvectors. Now the transfer function $\boldsymbol{H}_{\boldsymbol{FW}}(s)$ can be recast as

$$\boldsymbol{H}_{\boldsymbol{FW}}(s) = [\,\boldsymbol{H}_1(s) \quad \boldsymbol{H}_2(s) \quad \cdots \quad \boldsymbol{H}_{\bar{N}}(s)\,] \tag{39}$$

The time-domain realization of the transfer function $\boldsymbol{H}_{FW}(s)$ is needed for control system design and simulation. For this purpose, each column in matrix $\boldsymbol{H}_{FW}(s)$ is expressed in the following form [14]:

$$\boldsymbol{H}_i(s) = \frac{\boldsymbol{b}_i(s)}{a_i(s)}, \quad i = 1, 2, \ldots, \bar{N} \tag{40}$$

where

$$a_i(s) = s^n + a_i^{(1)} s^{n-1} + \cdots + a_i^{(n)} \tag{41}$$

$$\boldsymbol{b}_i(s) = \boldsymbol{b}_i^{(1)} s^{n-1} + \boldsymbol{b}_i^{(2)} s^{n-2} + \cdots + \boldsymbol{b}_i^{(n)} \tag{42}$$

$$\boldsymbol{H}_i(i\omega) = \boldsymbol{G}_i(\omega), \quad i = 1, 2, \ldots, \bar{N} \tag{43}$$

$$\boldsymbol{G}_i(\omega)\boldsymbol{G}_i^*(\omega) = \boldsymbol{\Psi}_i(\omega)\lambda_i(\omega)\boldsymbol{\Psi}_i^*(\omega) \tag{44}$$

If we let $\boldsymbol{F}_i(t)$ be the ith modal contribution to excitation process $\boldsymbol{F}_{bs}(t)$, then each function $\boldsymbol{H}_i(s)$ represents the transfer function from white noise to $\boldsymbol{F}_i(t)$. From Eq. (40), one obtains the following state-space model of the transfer function $\boldsymbol{H}_i(s)$:

$$\begin{cases} \dot{\boldsymbol{X}}_i = \boldsymbol{A}_i \boldsymbol{X}_i + \boldsymbol{B}_i w_i \\ \boldsymbol{F}_i(t) = \boldsymbol{C}_i \boldsymbol{X}_i \end{cases}, \quad i = 1, 2, \ldots, \bar{N} \tag{45}$$

where

$$\boldsymbol{A}_i = \begin{bmatrix} 0 & 1 & \cdots & 0 \\ \vdots & & \ddots & \\ 0 & 0 & & 1 \\ -a_i^{(n)} & -a_i^{(n-1)} & \cdots & -a_i^{(1)} \end{bmatrix}_{n\times n}, \qquad \boldsymbol{B}_i = \begin{bmatrix} 0 \\ \vdots \\ 0 \\ 1 \end{bmatrix}_{n\times 1} \tag{46}$$

$$\boldsymbol{C}_i = [\, \boldsymbol{b}_i^{(n)} \quad \boldsymbol{b}_i^{(n-1)} \quad \cdots \quad \boldsymbol{b}_i^{(1)} \,]_{N\times n} \tag{47}$$

Finally, we have the following state-space model of the random buffet loads:

$$\begin{cases} \dot{\boldsymbol{X}}_w(t) = \boldsymbol{A}_w \boldsymbol{X}_w(t) + \boldsymbol{B}_w \boldsymbol{W}_w(t) \\ \boldsymbol{F}_{bs}(t) = \boldsymbol{C}_w \boldsymbol{X}_w(t) \end{cases} \tag{48}$$

where

$$\boldsymbol{A}_w = \text{blockdiag}[\, \boldsymbol{A}_1 \quad \boldsymbol{A}_2 \quad \cdots \quad \boldsymbol{A}_{\bar{N}} \,] \tag{49}$$

$$\boldsymbol{B}_w = \text{blockdiag}[\, \boldsymbol{B}_1 \quad \boldsymbol{B}_2 \quad \cdots \quad \boldsymbol{B}_{\bar{N}} \,] \tag{50}$$

$$\boldsymbol{C}_w = [\, \boldsymbol{C}_1 \quad \boldsymbol{C}_2 \quad \cdots \quad \boldsymbol{C}_{\bar{N}} \,] \tag{51}$$

$$\boldsymbol{X}_w(t) = [\, \boldsymbol{X}_1^T \quad \boldsymbol{X}_2^T \quad \cdots \quad \boldsymbol{X}_{\bar{N}}^T \,]^T \tag{52}$$

$$\boldsymbol{W}_w(t) = [\, w_1 \quad w_2 \quad \cdots \quad w_{\bar{N}} \,]^T \tag{53}$$

V. Controller Design

Let us now consider the theoretical aspects of the active controller design. Because not all of the states of the system are measurable, suboptimal LQG control strategy is adopted. Next, the overall procedure used for the design of the active buffeting suppression system is also presented in the block diagram form.

A. Suboptimal Controller

From Eqs. (27) and (48), one can obtain the resulting open-loop aeroelastic equation of the vertical tail system:

$$\dot{\boldsymbol{X}}(t) = \boldsymbol{A}_{aw}\boldsymbol{X}(t) + \boldsymbol{B}_{av}\boldsymbol{V}_{\text{con}}(t) + \boldsymbol{B}_{aw}\boldsymbol{W}_w(t) \tag{54}$$

where

$$\boldsymbol{A}_{aw} = \begin{bmatrix} \boldsymbol{A}_a & \boldsymbol{D}_a\boldsymbol{\Phi}^T\boldsymbol{C}_w \\ \boldsymbol{0} & \boldsymbol{A}_w \end{bmatrix}, \qquad \boldsymbol{B}_{av} = \begin{bmatrix} \boldsymbol{B}_a \\ \boldsymbol{0} \end{bmatrix} \tag{55}$$

$$\boldsymbol{B}_{aw} = \begin{bmatrix} \boldsymbol{0} \\ \boldsymbol{B}_w \end{bmatrix}, \qquad \boldsymbol{X}(t) = \begin{Bmatrix} \boldsymbol{X}_a(t) \\ \boldsymbol{X}_w(t) \end{Bmatrix} \tag{56}$$

With the purpose of reducing vibrations of the vertical tail, one can establish a feedback control loop in which the signals from sensors are fed back to the piezoelectric actuators. Because not all of the state components are always available for feedback purpose in practical applications, the output feedback with partial states is used here. Measured velocity output $\boldsymbol{Y}_{ae}(t)$ from sensors are directly fed back to actuators through

$$\boldsymbol{Y}_{ae}(t) = \boldsymbol{C}_{aw}\boldsymbol{X}(t) \tag{57}$$

where

$$\boldsymbol{C}_{aw} = \boldsymbol{S}_v\boldsymbol{\Phi}[\, \boldsymbol{0}_{n_r\cdot n_r} \quad \boldsymbol{I}_{n_r\cdot n_r} \quad \boldsymbol{0}_{n_r\cdot n_a} \quad \boldsymbol{0}_{n_r\cdot n_w} \,] \tag{58}$$

where $\boldsymbol{S}_v$ is the matrix for which the elements are related to the locations of sensors, n_r is the number of the retained modes, and n_w are the dimensions of the state vector $\boldsymbol{X}_w(t)$.

Suboptimal control law is given by

$$\boldsymbol{V}_{\text{con}}(t) = -\boldsymbol{K}_{\text{con}}\boldsymbol{Y}_{ae}(t) \tag{59}$$

where the control gain $\boldsymbol{K}_{\text{con}}$ is determined by

$$\boldsymbol{K}_{\text{con}} = \boldsymbol{F}^*\boldsymbol{C}_{aw}^T(\boldsymbol{C}_{aw}\boldsymbol{C}_{aw}^T)^{-1} \tag{60}$$

$$\boldsymbol{F}^* = \bar{\boldsymbol{R}}^{-1}\boldsymbol{B}_{av}^{-1}\boldsymbol{P} \tag{61}$$

$$\boldsymbol{A}_{aw}^T\boldsymbol{P} + \boldsymbol{P}\boldsymbol{A}_{aw} - \boldsymbol{P}\boldsymbol{B}_{av}\bar{\boldsymbol{R}}^{-1}\boldsymbol{B}_{av}^T\boldsymbol{P} + \bar{\boldsymbol{Q}} = \boldsymbol{0} \tag{62}$$

where $\bar{\boldsymbol{R}}$ and $\bar{\boldsymbol{Q}}$ are the control penalty and state penalty matrix, respectively.

Application of negative velocity feedback introduces damping into the system by altering the eigenvalues of the following closed-loop system:

$$\dot{\boldsymbol{X}}(t) = (\boldsymbol{A}_{aw} - \boldsymbol{B}_{av}\boldsymbol{K}_{\text{con}}\boldsymbol{C}_{aw})\boldsymbol{X}(t) + \boldsymbol{B}_{aw}\boldsymbol{W}_w(t) \tag{63}$$

B. Block Diagram of the System

Figure 2 depicts the block diagram of active buffeting suppression system. First, the combined structure is discretized by solid finite elements in ANSYS. In this step, the piezoelectric constitutive law is included in the element formulation for the actuators. Then the finite element model for both of the vertical tail and the piezoelectric actuators are imported into MATLAB. To reduce the amount of memory required for data storage, the system matrices are stored in sparse matrices format. On the basis of the node table and degree of freedom (DOF) table, matrix partition operations are performed to separate the structural DOF and electric potential DOF. Afterward, the nodes modeling the electrode surface of each actuator have their voltage DOF coupled so that the applied potential load can be conveniently placed on a single node. Now modal analysis of the

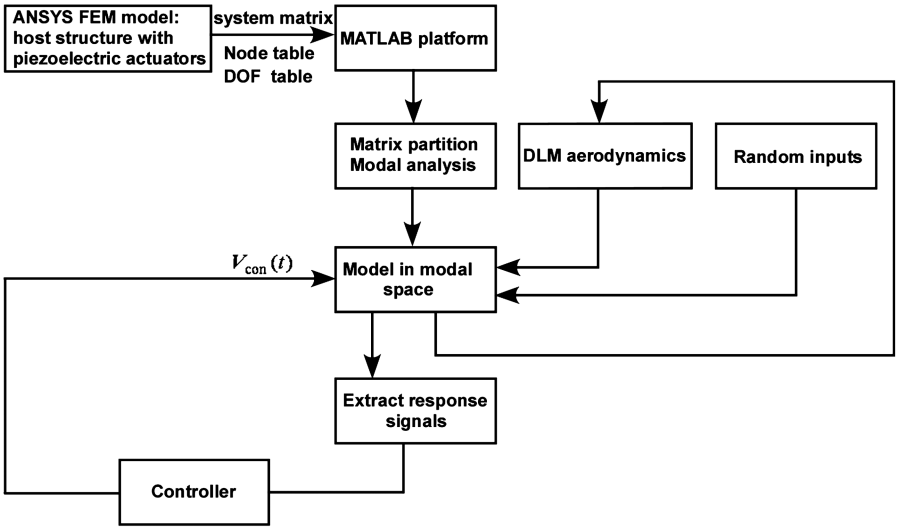

Fig. 2 Block diagram of the active buffeting suppression system.

system can be performed in MATLAB to form the structural dynamical equations in modal space. As shown in Fig. 2, the total aerodynamic forces on the vertical wing can be represented by the addition of the motion-induced aerodynamic forces and the random buffet loads. The motion-induced aerodynamic forces can be modeled by using DLM, and the random buffet loads can be modeled by the POD method for the given PSD matrix of the aerodynamic loads on the rigid-vertical-tail model. For the control procedure, the signals from sensors are fed back into the designed controller, and then the suboptimal control voltages on piezoelectric patches are computed. Because of the inverse piezoelectric effect of the actuators, the buffeting of the vertical tail is attenuated.

VI. Numerical Results

The material of the vertical tail is assumed to be aluminum and isotropic. Young's modulus of elasticity is $E_e = 40$ GPa, Poisson's ratio is $v = 0.33$, and the density is $\rho = 2765.0$ kg/m^3. As shown in Fig. 3, the vertical tail is modeled using solid elements (SOLID45); each SOLID45 elements has 8 nodes and 24 DOF. The vertical tail consists of a total of $28 \times 28 = 784$ SOLID45 elements. Nine PIC141 piezoelectric patches are perfectly bonded on one side of the vertical tail. The adhesive layers are neglected. In ANSYS platform, the most suitable element having piezoelectric capability in the three-dimensional coupled field problems is the solid-type element SOLID5. Similar to other structural solid elements, SOLID5 element has eight nodes, and each node has three displacement DOF. In addition to these DOF, the element also has potential DOF for the analysis of the electromechanical coupling problems.

The material properties of PIC141 patches have been used to form the following input matrices:

$$\boldsymbol{C} = \begin{bmatrix} 12.4 & 7.0 & 7.4 & 0 & 0 & 0 \\ & 12.4 & 7.4 & 0 & 0 & 0 \\ & & 13.0 & 0 & 0 & 0 \\ \text{sym} & & & 2.8 & 0 & 0 \\ & & & & 2.9 & 0 \\ & & & & & 2.9 \end{bmatrix} \times 10^{10} \text{ Pa} \tag{64}$$

$$\boldsymbol{e} = \begin{bmatrix} 0 & 0 & -4.2 \\ 0 & 0 & -4.2 \\ 0 & 0 & 19.6 \\ 0 & 0 & 0 \\ 0 & 13.8 & 0 \\ 13.8 & 0 & 0 \end{bmatrix} \text{C/m}^2 \tag{65}$$

$$\boldsymbol{\varepsilon}^S = \begin{bmatrix} 13.281 & 0 & 0 \\ 0 & 13.281 & 0 \\ 0 & 0 & 11.510 \end{bmatrix} \times 10^{-9} \text{ F/m} \tag{66}$$

The natural frequencies and the corresponding modal shapes of the vertical tail are shown in Fig. 4. To test the driving capability of the piezoelectric patches and the correctness of the finite element model (FEM), constant voltages of +600 and −600 V are applied to the

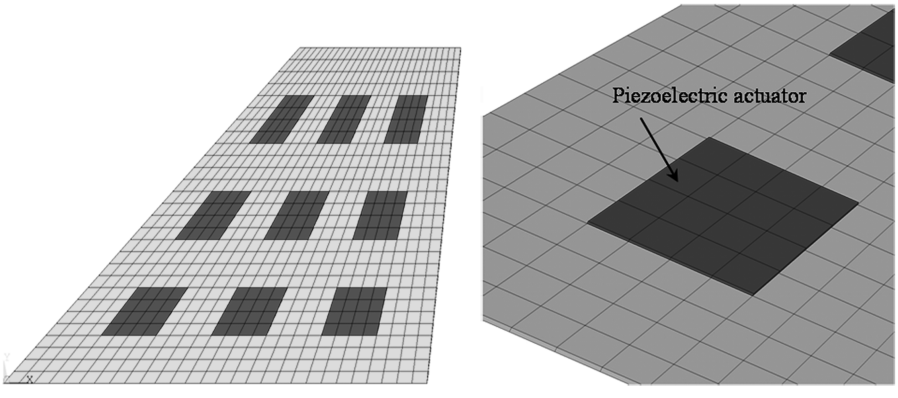

Fig. 3 FEM of the vertical tail structure.

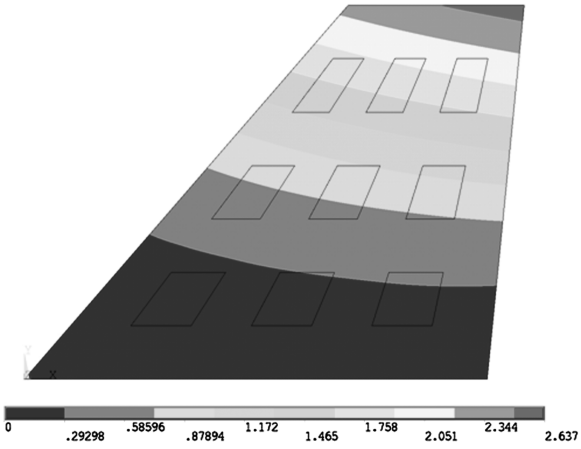

a) The first mode (9.807 Hz)

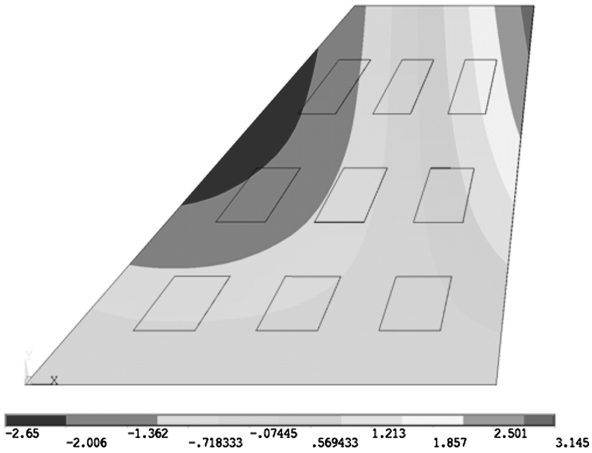

b) The second mode (34.66 Hz)

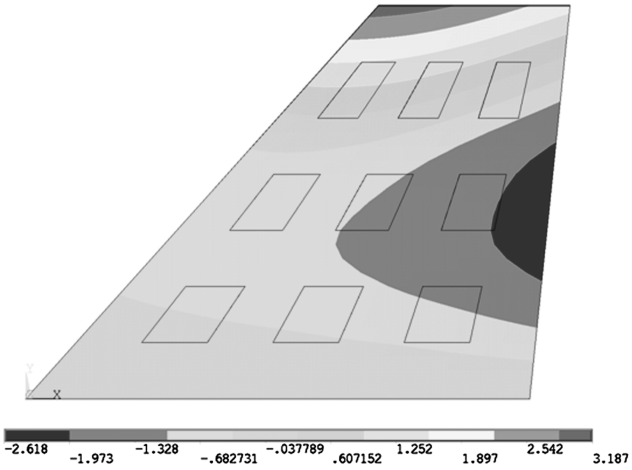

c) The third mode (55.032 Hz)

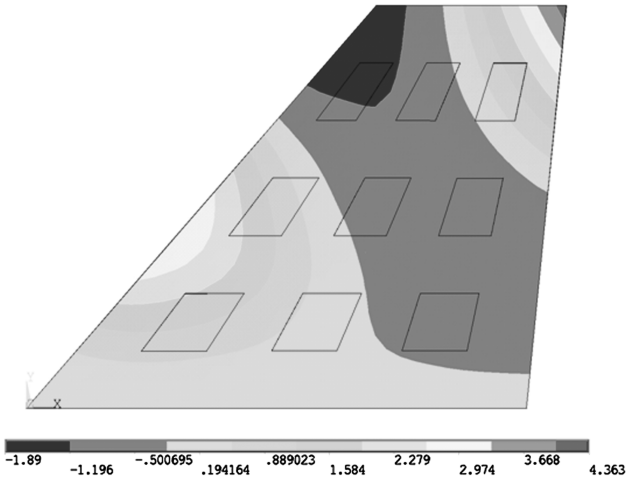

d) The fourth mode (87.632 Hz)

Fig. 4 Modal shapes and natural frequencies of the vertical tail.

piezoelectric patches, respectively. The induced deformations of the vertical tail are shown in Fig. 5.

In the procedure of the structural modeling, the first six modes of the vertical tail are retained. In the motion-induced aerodynamic modeling, generalized aerodynamic matrices are computed at a total of 20 reduced frequency points in the interval [0.001, 1.0]. To transform the unsteady aerodynamic forces into state space in the time domain, the minimum state method is used to approximate the generalized aerodynamic in the Laplace domain. Figure 6 presents a plot showing the approximation of unsteady generalized aerodynamic forces. Based on the POD method, the random buffeting loads are treated as the outputs of a state-space model under white-noise inputs [see Eq. (48)]. Up to now, the resulting aeroelastic equations of the vertical tail/piezoelectric patch system are formed in

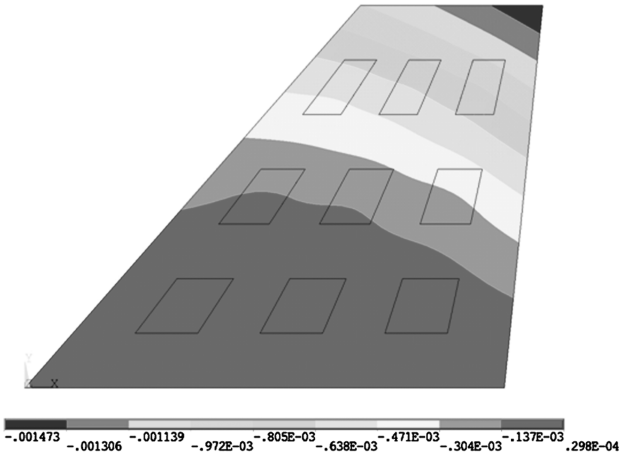

a) 600 V

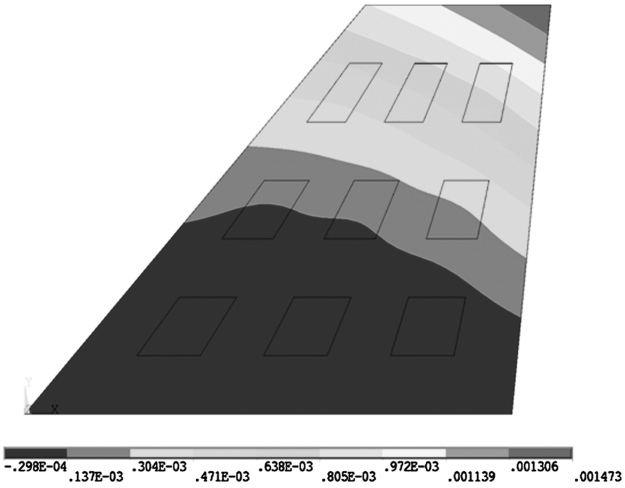

b) -600 V

Fig. 5 Static deformation of the vertical tail under constant voltage.

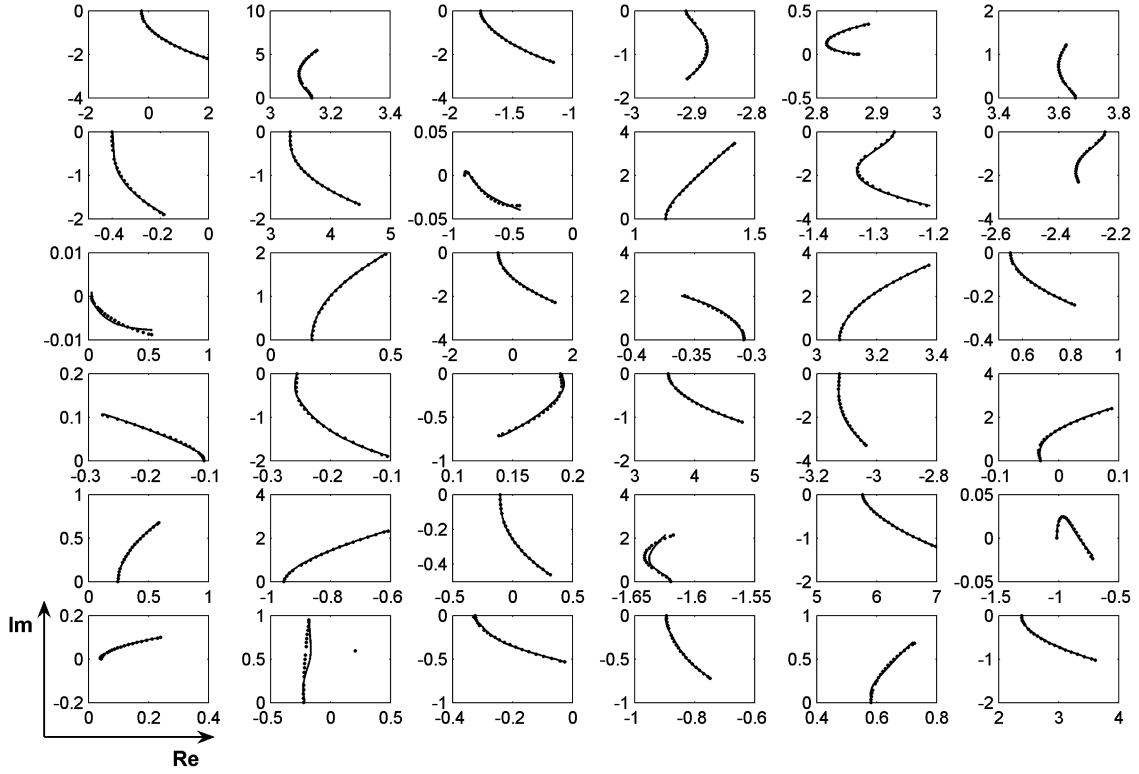

Fig. 6 Generalized aerodynamic forces: DLM (lines) and approximated values (circles).

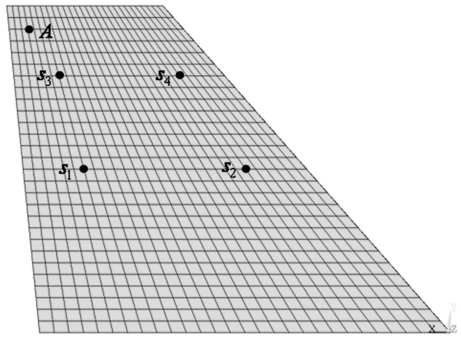

Fig. 7 Response monitoring point and feedback measuring points s_1–s_4.

the time domain, and the controller can be further designed by suboptimal control theory.

The simulation flow speed is taken as $V_\infty = 50$ m/s and Mach number is $M_\infty = 0$. As shown in Fig. 7, the velocity signals in the z direction of the tail are taken as the feedback signals. The free

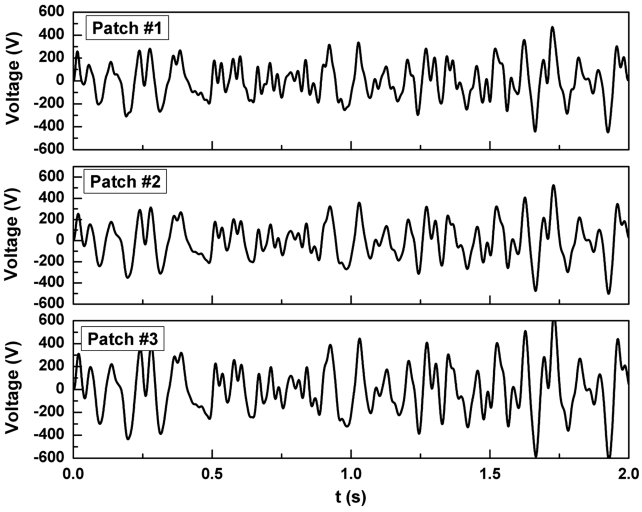

Fig. 9 Time histories of the control voltages (actuators 1–3).

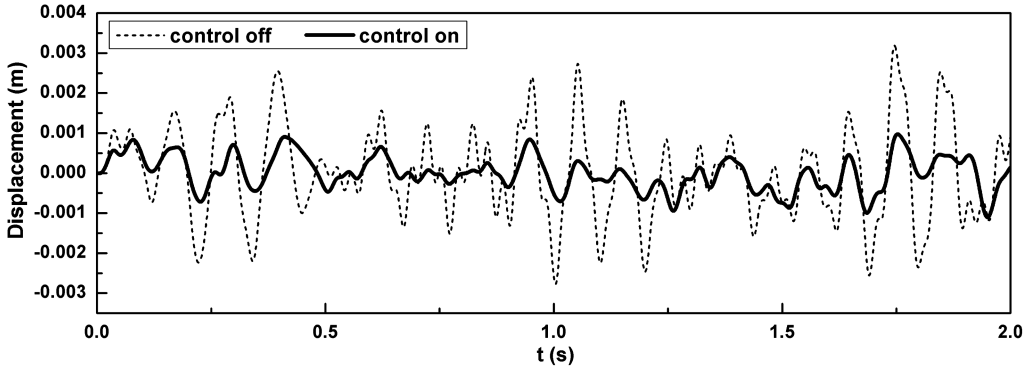

Fig. 8 Displacement response of node A.

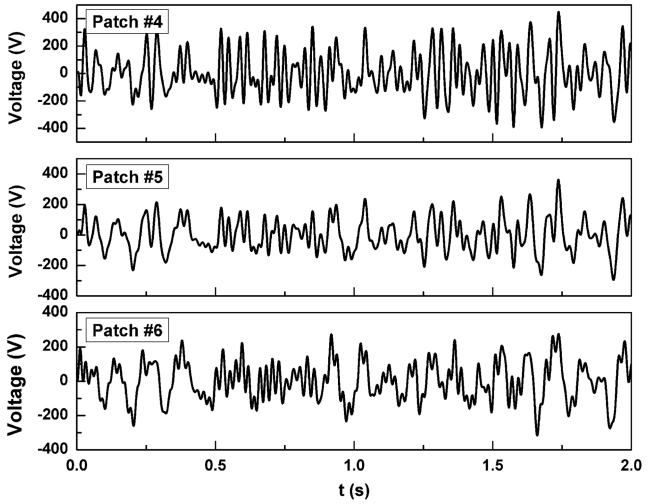

Fig. 10 Time histories of the control voltages (actuators 4–6).

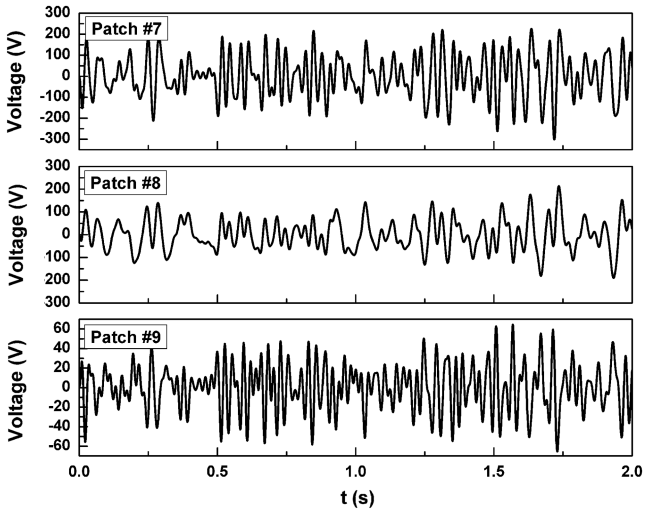

Fig. 11 Time histories of the control voltages (actuators 7–9).

parameters $\bar{\boldsymbol{R}}$ and $\bar{\boldsymbol{Q}}$ are determined by trial-and-error method to most effectively control the structure. Once the suboptimal controller design is completed, the closed-loop simulation can be performed to test the performance of the controller. Displacement responses of node A are shown in Fig. 8. Results when the control is off are also shown for comparison. Actuator voltages are shown in Figs. 9–11. As can be seen, the buffeting of the vertical tail is significantly suppressed by using the suboptimal controller.

VII. Conclusions

A simplified method is present and demonstrated for using piezoelectric actuators to reduce the buffeting responses of a vertical tail. The proposed scheme features the simplified modeling procedure for buffet loads and the interaction between ANSYS and MATLAB platforms. Numerical results indicate that the efficient buffeting suppression can be achieved using bonded piezoelectric patches.

Acknowledgment

The work was supported by the National Natural Science Foundation of China under grant 10825207.

References

[1] Hauch, R. M., "Reduction of Vertical Tail Buffet Response Using Active Control," *Journal of Aircraft*, Vol. 33, No. 3, 1996, pp. 617–622. doi:10.2514/3.46990

[2] Bean, D. E., Greenwell, D. I., and Wood, N. J., "Vortex Control Technique for the Attenuation of Fin Buffet," *Journal of Aircraft*, Vol. 30, No. 6, 1993, pp. 847–853. doi:10.2514/3.46426

[3] Bean, D. E., and Wood, N. J., "Experimental Investigation of Twin-Fin Buffeting and Suppression," *Journal of Aircraft*, Vol. 33, No. 4, 1996, pp. 761–767. doi:10.2514/3.47012

[4] Lazarus, K. B., Saarmaa, E., and Agnes, G. S., "Active Smart Material System for Buffet Load Alleviation," *Proceedings of SPIE: The International Society for Optical Engineering*, Vol. 2447, 1995, pp. 179–192. doi:10.1117/12.209331

[5] Spangler, R. L., and Jacques, R. N., "Testing of An Active Smart Material System for Buffet Load Alleviation," AIAA Paper 1999-1317, 1999.

[6] Hauch, R. M., Jacobs, J. H., Ravindra, K., and Dima, C., "Reduction of Vertical Tail Buffet Response Using Active Control," *Journal of Aircraft*, Vol. 33, No. 3, 1996, pp. 617–622. doi:10.2514/3.46990

[7] Nitzsche, F., Zimcik, D. G., and Langille, K., "Active Control of Vertical Fin Buffeting with Aerodynamic Control Surface and Strain Actuation," AIAA Paper 1997-1386, 1997.

[8] Nitzsche, F., Zimcik, D. G., and Ryall, T. G., "Control Law Synthesis for Vertical Fin Buffeting Alleviation Using Strain Actuation," AIAA Paper 1999-1317, 1999.

[9] Moses, R. W., "Vertical-Tail-Buffeting Alleviation Using Piezoelectric Actuators: Some Results of the Actively Controlled Response of Buffet-Affected Tails (ACROBAT) Program," *Proceedings of SPIE: The International Society for Optical Engineering*, Vol. 3044, 1997, pp. 87–98. doi:10.1117/12.274700

[10] Sheta, E. F., and Moses, R. W., "Active Smart Material Control System for Buffet Alleviation," *Journal of Sound and Vibration*, Vol. 292, 2006, pp. 854–868. doi:10.1016/j.jsv.2005.09.002

[11] Lee, B. H. K., "Statistical Analysis of Wing/Fin Buffeting Response," *Progress in Aerospace Sciences*, Vol. 38, 2002, pp. 305–345. doi:10.1016/S0376-0421(02)00007-6

[12] Albano, E., and Rodden, W. P., "A Doublet-Lattice Method for Calculating Lift Distributions of Oscillating Surfaces in Subsonic Flow," *AIAA Journal*, Vol. 7, No. 2, 1969, pp. 279–285. doi:10.2514/3.5086

[13] Benfratello, S., and Muscolino, G., "Filter Approach to the Stochastic Analysis of MDOF Wind-Excited Structures," *Probabilistic Engineering Mechanics*, Vol. 14, 1999, pp. 311–321. doi:10.1016/S0266-8920(98)00041-1

[14] Carassale, L., "POD-Based Filters for the Representation of Random Loads on Structures," *Probabilistic Engineering Mechanics*, Vol. 20, 2005, pp. 263–280. doi:10.1016/j.probengmech.2005.05.008